Decreased expression of PBLD correlates with poor prognosis and functions as a tumor suppressor in human hepatocellular carcinoma

Supplementary Material

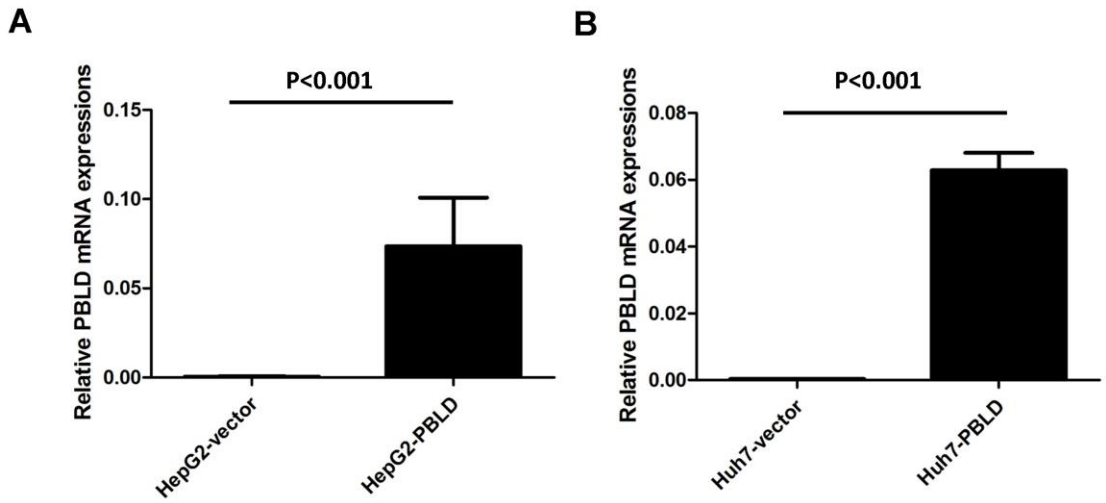

Supplementary Fig. 1. PBLD mRNA expression was significantly up-regulated in HepG2 and Huh7 cell lines after transfection detected by qRT-PCR. The expression level of PBLD was up-regulated 216-fold, 198-fold ($p < 0.01$) in HepG2_PBLD (A) and Huh7_PBLD (B) cell lines, respectively, compared with control pEGFP-N1 vector transfected cells.

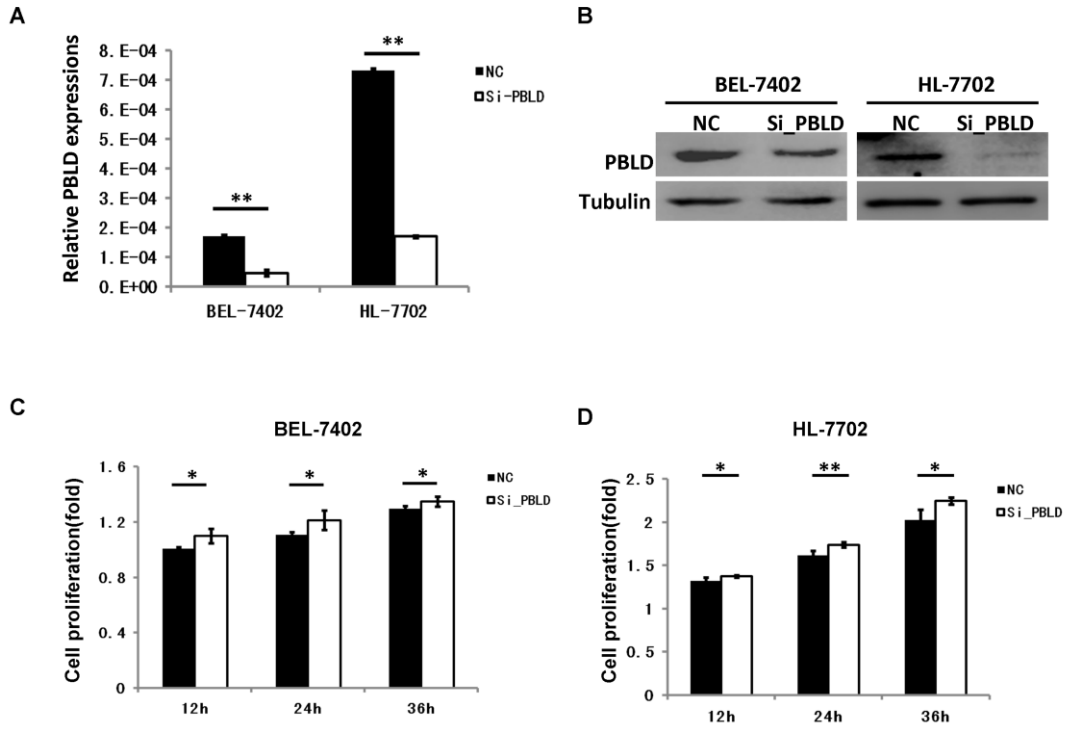

Supplementary Fig. 2. PBLD downregulation significantly enhanced the proliferation rate of HCC cells in vitro. (A) BEL-7402 and HL-7702 cell-lines transfected with PBLD siRNA or empty vector, PBLD mRNA expressions of BEL-7402 and HL-7702 cell-lines were efficiently downregulated after transfection as detected by qRT-PCR (P<0.001). (B) PBLD protein expressions of BEL-7402 and HL-7702 cell-lines were efficiently downregulated after transfection as detected by western blotting. (C, D) PBLD downregulation enhanced cell proliferation *in vitro* as analyzed by the cck-8 assay in BEL-7402 and HL-7702 cell-lines respectively. (*P<0.05, **P<0.01)

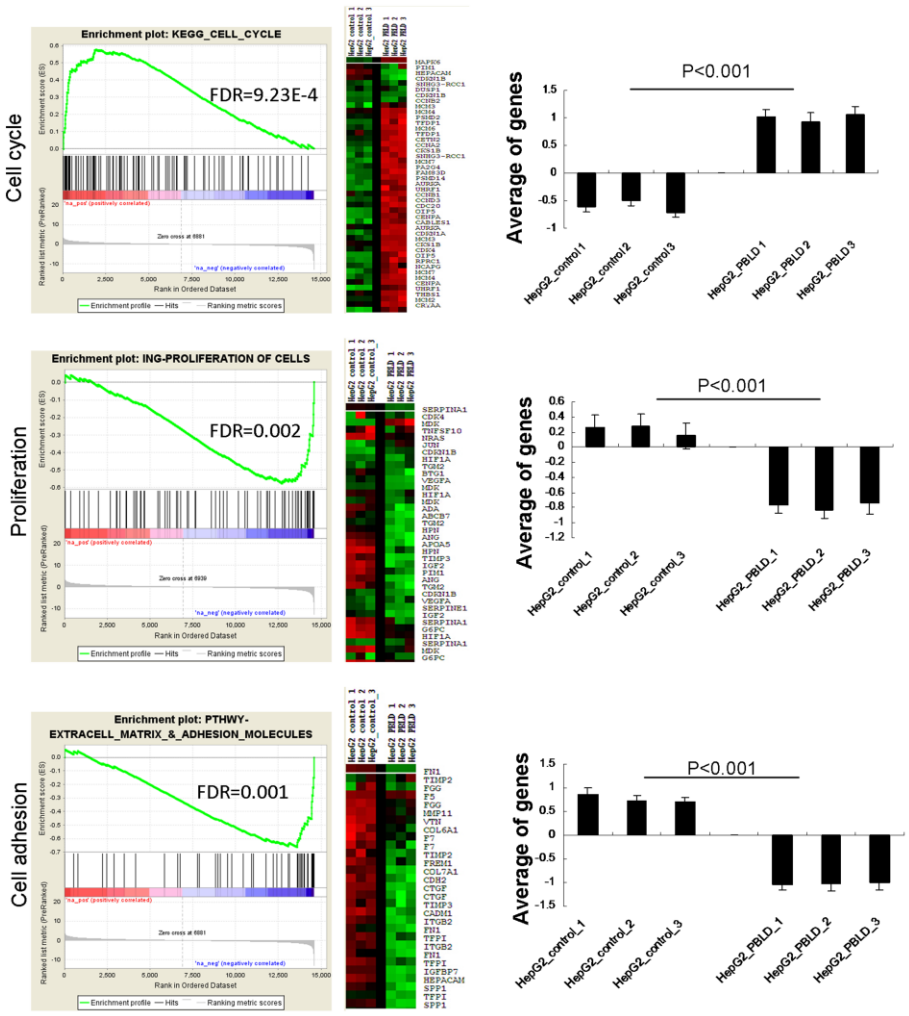

Supplementary Fig. 3.Cell cycle, proliferation and cell adhesion pathway related genes showed a marked deregulation in PBLD_HepG2 cells compared with control. GSEA results for all fold changes calculated, the cell cycle (A), proliferation (B) and cell adhesion (C) pathway were all significantly deregulated; Heatmap displayed significant gene expression; the average gene expression for each sample in group were calculated (P<0.001).

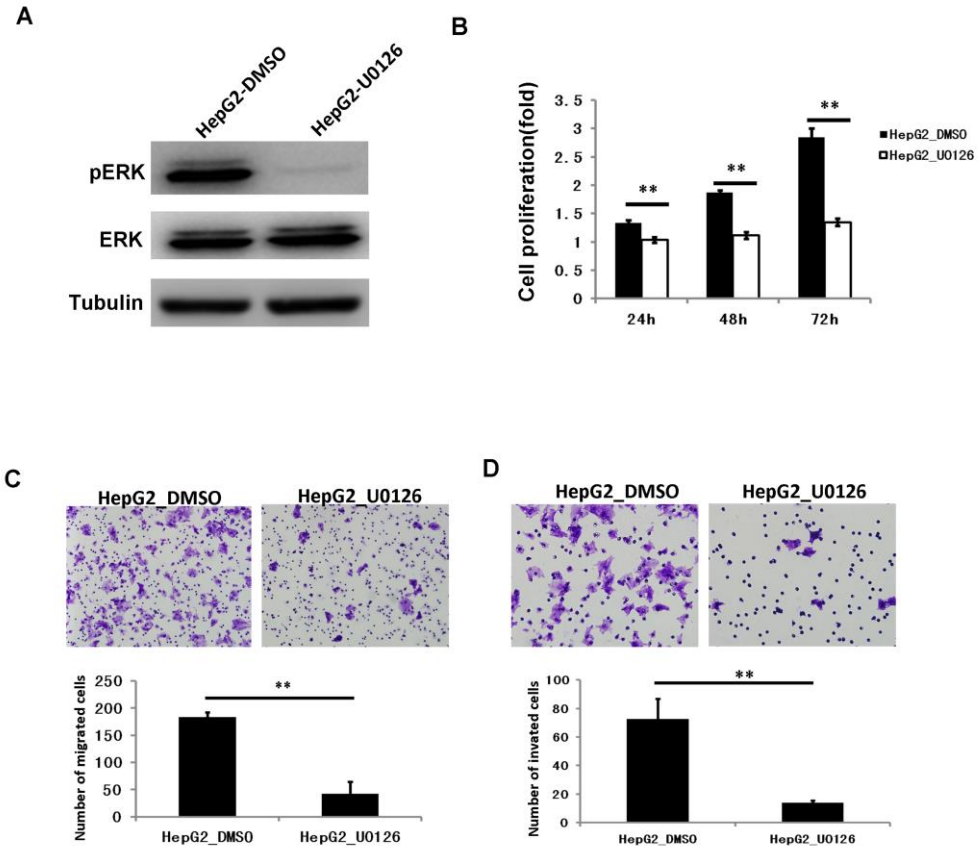

Supplementary Fig. 4. Impairment of ERK1/2 pathways inhibited proliferation, migration and invasion of HepG2 cell lines *in vitro* as similar as those induced by PBLD overexpression. (A) phospho-ERK protein expressions of HepG2 were efficiently downregulated after treated with U0126 as detected by western blotting. (B) Impairment of ERK1/2 pathways inhibited cell proliferation *in vitro* as analyzed by the cck-8 assay (P<0.001). (C, D) impairment of ERK1/2 pathways in HepG2 resulted in inhibition of cell migration and invasion *in vitro* (P<0.001).

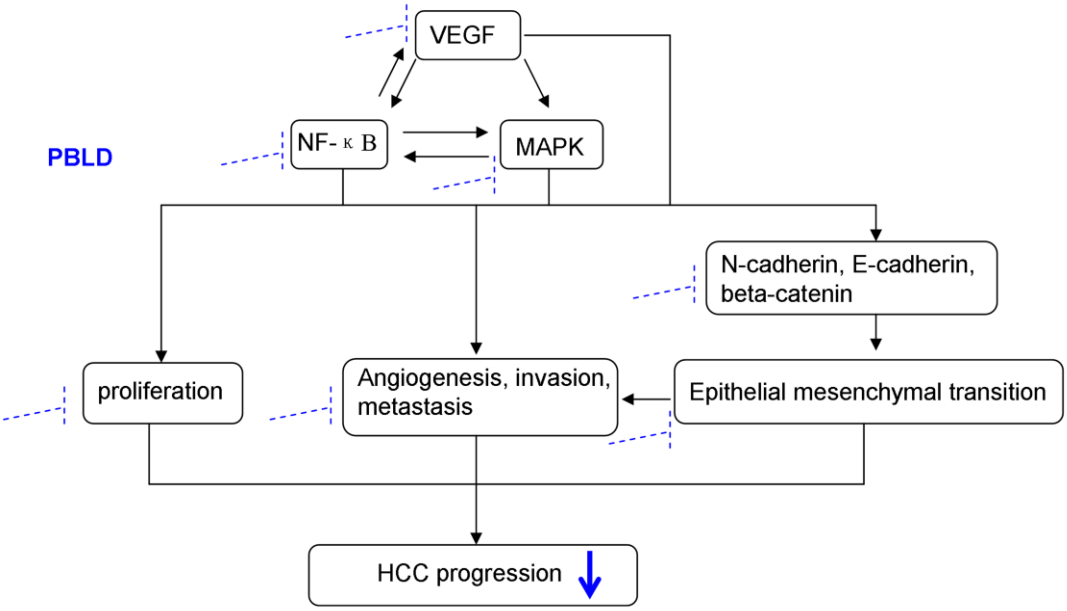

Supplementary Fig. 5.Several molecular mechanisms of PBLD have been recognized which involved in the progression of HCC. Elevated PBLD expression may reduce HCC growth and metastasis through inactivation of several tumorigenesis-related signaling pathways, including angiogenesis/VEGF, EMT, NF-κB, MAPK.

Supplementary Methods

Immunohistochemical assay

IHC staining for PBLD expression was done on 4-μm sections from paraffin-embedded tissue specimens. The sections were deparaffinized in xylene, and rehydrated by a series of graded ethanol rinse. Masked epitope retrieval was done by heating the sections in a microwave oven in 0.01 M sodium citrate buffer (pH 6.0) for 20 min to retrieve antigens. Endogenous peroxidase activity was terminated by incubation in 3% H_2O_2 for 20 min at room temperature. The sections were then incubated at 4ºC overnight with PBLD monoclonal mouse anti-human IgG (Santa Cruz Biotechnology, Santa Cruz, CA, USA) or CD31 polyclonal rabbit anti-human IgG (1:50; Abcam, Cambridge, UK) in a 1:50 dilution with 5% skimmed milk PBS buffer. Incubations with corresponding secondary antibodies were performed after the sections were allowed to stay at room temperature for 45 min. The antibody-antigen complexes were visualized with diaminobenzidine (DAB) alone and counterstained with haematoxylin. Finally, the sections were dehydrated in ethanol, cleared in xylene, and examined under light microscopy. Sections known to show positive staining for PBLD were included in each run, receiving either the primary antibody or PBS, as positive or negative controls. In all staining procedures, the positive controls showed clear staining, whereas there was no staining in the negative controls. For indirect immunofluorescence assay, the primary antibodies anti-PBLD monoclonal antibody (Santa Cruz Biotechnology, Santa Cruz, CA, USA) and anti-VEGF monoclonal antibody (Bioworld technology, co, Ltd, Nanjing, China) and secondary

antibody Cy3-goat anti-rabbit-IgG (EarthOx Life Science, Millbrae, CA, USA) were used.

The IHC slides were analyzed by three independent investigators without knowledge of clinicopathologic or biological information, one of whom was experienced pathologist (S. Liu). Every sample was given a score according to the intensity of the staining (no staining = 0, weak staining = 1, moderate staining = 2, strong staining = 3) and the extent of stained cells (<5% = 0, 5%–25% = 1, 26%–50% = 2, 51%–75% = 3, 76%–100% = 4). The percentage of cells at each intensity was multiplied by the corresponding intensity value to obtain an immunostaining score ranging from 0 to 12. The scores were combined to obtain an overall mean score. Using this assessment system, optimal cutoff values were identified by the mean score as follows: 0–3 (low), 4–8–12 (high). For quantification of angiogenesis, CD31-positive areas were counted at high power magnification in 15 random fields. Data was collected by two independent observers and the number of CD31-positive vessels was taken as the microvessel density (MVD) of individual groups.

Western blotting

Protein was extracted in RIPA buffer (Millipore, Billerica, MA, USA) containing 1% Halt Protease and Phosphatase Inhibitor Cocktails (Thermo Scientific, Rockford, IL, USA). The concentration of protein was determined using Pierce BCA Protein Assay Kit (Thermo Scientific, Rockford, IL, USA). Samples with equal amounts of total protein were separated by 12% SDS-PAGE and electrotransferred from the gel to

PVDF membranes (Bio-Rad Laboratories, Hercules, CA, USA). After blocking with 5% BSA (Sigma-Aldrich, St. Louis, MO, USA) in Tris-buffered saline (TBS) with 0.05% Tween-20 (Sigma-Aldrich, St. Louis, MO, USA) for 1 hour at room temperature with shaking, the membranes were probed subsequently by the primary antibodies mouse-anti-PBLD (1:1000; Abcam, Cambridge, UK), phospho-ERK (1:1000; Cell Signaling Technology, Inc, Beverly, MA; USA), total ERK (1:1000; Cell Signaling Technology, Inc, Beverly, MA; USA), phospho-p38 (1:1000; Cell Signaling Technology, Inc, Beverly, MA; USA), total p-38 (1:1000; Cell Signaling Technology, Inc, Beverly, MA; USA), phospho-JNK (1:1000; Cell Signaling Technology, Inc, Beverly, MA; USA), total JNK (1:1000; Cell Signaling Technology, Inc, Beverly, MA; USA), phospho-NF-κB (1:1000; Cell Signaling Technology, Inc, Beverly, MA; USA), total NF-κB (1:1000; Cell Signaling Technology, Inc, Beverly, MA; USA), VEGF-A (1:500; Bioworld technology, co, Ltd, Nanjing, China), E-cadherin (1:750; Bioworld technology, co, Ltd, Nanjing, China), N-cadherin (1:1000; Bioworld technology, co, Ltd, Nanjing, China), β-catenin (1:500; Bioworld technology, co, Ltd, Nanjing, China) at 4°C overnight. Tubulin (Tianjin Sungene Biotech Co., Ltd, Tianjin, China) or GAPDH (Tianjin Sungene Biotech Co., Ltd, Tianjin, China) was used as an internal control.

Quantitative real-time PCR

Total RNA was extracted from tissues using TRIZOL (Invitrogen Life Technologies Inc., Gaithersburg, USA) according to the manufacturer's protocol. One microgram of total RNA was reverse transcribed using a standard oligo

(deoxythymidine) primer in a total volume of 20 μl. Thirty nanogram of cDNA from each sample was used as template for PCR amplification with specific oligonucleotide primers in the Roche LightCycler 480 Real Time PCR System (Roche Diagnostics, Mannheim, Germany). PCR reactions were performed according to the manufacturer's instructions, using the SYBR Green qPCR Master Mix (DBI Bioscience, Shanghai, China). The following conditions were used for PCR: 95 °C for 15 s, 60°C for 20 s and repeated for 40 cycles. The identities of the PCR products were confirmed by melting temperatures and dissociation curves. For quantitation of gene expression, the fluorescence of the SYBR Green dye bound to the PCR products was measured after each cycle, and the cycle numbers were recorded when the accumulated signals crossed an arbitrary threshold (CT value). All PCR reactions were performed in duplicate when cDNA samples were available. To normalize this value, a ΔCT value was determined as the difference between the CT value for each gene and the CT value for GAPDH. For each gene, a ΔΔCT value was determined as the difference between the ΔCT value for each HCC tissue sample and the average ΔCT value for this gene obtained from the normal tissue samples. These ΔΔCT values were then used to calculate $2^{-\Delta\Delta CT}$ values as relative gene expression. The primer sequences for real-time PCR were as follows: PBLD sense, 5'- GGGTCTGCACACG CTGTTC-3' and antisense, 5'- TAATGTCAACCCTTCCGTCT -3'; JUN sense, 5'- CCAAAGGATAGTGCGATGTTT -3' and antisense, 5'- CTGTCCCTCTCCA CTGCAAC -3', E-cadherin sense, 5'- GAGTGCCAACTGGACCATTCAGTA -3' and antisense, 5'- AGTCACCCACCTCTAAGGCCATC -3', N-cadherin sense, 5'-

CGAATGGATGAAAGACCCATCC-3' and antisense, 5'- GGAGCCACTGCCTTC ATAGTCAA-3', beta catenin sense, 5'- GCTTGTTCGTGCACATCAGGATA -3' and antisense, 5'- GGCTCCGGTACAACCTTCAACTA-3, GAPDH sense, 5'- GAAGGT GAAGGTCGGAGT-3' and antisense, 5'-GAAGATGGTGATGGGATTTC-3'.

Microarray analysis

Total RNA was extracted using the Trizol Reagent method. Additional purification was performed on RNeasy columns (Qiagen, Valencia, CA 913555, cat. no. 74104). The quality of total RNA samples as assessed using an Agilent 2100 Bioanalyzer (Agilent Technologies, Palo Alto, CA).

RNA samples were labeled according to the chip manufacturer's recommended protocols. In brief, for Illumina, 0.5 µg of total RNA from each sample was labeled by using the IlluminaTotalPrep RNA Amplification Kit (Ambion, Austin, TX 78744-1832, cat. no. IL1791) in a two step process of cDNA synthesis followed by *in vitro* RNA transcription. Single stranded RNA (cRNA) was generated and labeled by incorporating biotin-16-UTP. 0.75 µg of biotin-labeled cRNA was hybridized (16 hours) to Illumina HumanHT-12_v4 BeadChips (Illumina, San Diego, CA, USA). The hybridized biotinylated cRNA was detected with streptavidin-Cy3 and quantified using Illumina'sBeadStation 500GX Genetic Analysis Systems scanner.

Preliminary data analysis of the scanned data was performed using IlluminaBeadStudio software which returned single intensity data values/gene following the computation of a trimmed mean average for each probe type

represented by a variable number of bead probes/gene on the array. Z-transformation for normalization was performed on each Illumina sample/array on a stand-alone basis, and significant changes in gene expression between class pairs were calculated by Z test. Significant gene lists were calculated by selecting genes which satisfied a significance threshold criteria of Z test p-values less than or equal to 0.001 (10^{-3}), a false discovery rate less than or equal to 0.1, and a fold change ± 1.5 or greater.

Supplementary Table1. The clinicopathological characteristics of 90 patients with HCC in the validated cohort.

Variables	**No. of patients(n=90)**
Median age (y; range)	54(25-73)
Gender	
Male	78
Female	12
Liver Cirrhosis	
Absent	56
Present	34
Vascular invasion	
Absent	82
Present	8
Intrahepatic metastasis	
Absent	78
Present	11
Tumor size	
≤5 cm	38
＞5 cm	51
Tumor number	
Single	78
Multiple	11
Tumor differentiation	
Well- Moderate	56
Poor	34
TNM stage	
I/II	45
III/IV	45

Table Legend: A total of 90 HCC samples on the TMA with clinicopathological characteristics listed above were used as an independent validation cohort.

Supplementary Table2. Univariate and multivariate analyses in the validated patients cohort.

	RFS		OS	
	HR (95%CI)	***P* value**	**HR (95%CI)**	***P* value**
Univariate analysis				
Age, yrs (<50 vs. ≥50)	0.987 (0.963-1.011)	0.291	0.993 (0.967-1.018)	0.568
Gender (male vs. female)	1.041 (0.495-2.188)	0.916	1.135 (0.537-2.397)	0.740
Liver cirrhosis (absent vs. present)	0.965 (0.576-1.618)	0.892	0.917 (0.535-1.570)	0.751
Vascular invasion (absent vs. resent)	2.547 (1.146-5.661)	**0.022**	3.002 (1.341-6.724)	**0.008**
Intrahepatic metastasis (absent vs. present)	1.659 (0.814-3.381)	0.163	1.734 (0.848-3.548)	0.132
Tumor size, cm (≤5 vs. >5)	2.089 (1.225-3.562)	**0.007**	2.157 (1.245-3.801)	**0.006**
Tumor number (single vs. multiple)	1.659 (0.814-3.381)	0.163	1.734 (0.848-3.548)	0.132
Differentiation (poor/moderate vs. well)	1.281 (0.770-2.129)	0.341	1.305 (0.773-2.202)	0.319
AJCC stage(I-II vs. III-IV)	2.505 (1.492-4.205)	**0.001**	2.552 (1.486-4.385)	**0.001**
PBLD (low vs. high)	0.522 (0.309-0.882)	**0.015**	0.563 (0.329-0.965)	**0.037**
Multivariate analysis				
AJCC stage (I-II vs. III-IV)	2.052 (1.065-3.953)	**0.032**	1.982 (1.006-3.905)	**0.048**
PBLD (low vs. high)	0.490 (0.285-0.841)	**0.010**	0.528 (0.303-0.922)	**0.025**

Table Legend: Univariate and multivariate analysis showed that PBLD was a prognostic predictor for both RFS and OS in another independent patients cohort.

Supplementary Table 3. Effects of PBLDoverexpression on cell cycle distribution in HepG2 and Huh7 cell lines by flow cytometry.

Groups	G0-G1 (%)	S phase (%)	G2/M (%)
Huh7-vector	67.28±0.76	23.36±2.36	9.31±3.05
Huh7-PBLD	50.73±1.86**	39.52±3.13**	9.93±3.30
HepG2-vector	59.98±2.76	22.42±2.21	17.60±0.62
HepG2-PBLD	46.53±0.99**	21.98±0.42	31.49±0.61**

NOTE: Values were presented as mean ± SD of three independent experiments. **P<0.01, compared to the corresponding vector-expressing transfectants.

Table Legend: Cell cycle analysis revealed that PBLD overexpression caused a considerable inhibition of cell cycle progression, a characteristic decreased G1 phase, leading to a selective accumulation of cells in the S phase compared with control in Huh7 cells and G2/M phase arrest in HepG2 cells.

Supplementary Table 4. Genes showing significantly different expression level regulated by PBLD overexpression in HepG2 cells.

Function	Gene symbol	Gene name	Expression change in HCC tumor*	GenBank No.	UniGene ID
NF-κB	**LGALS1**	Lectin, galactoside-binding, soluble, 1	↓	NM_002305.3	Hs.445351
	TGM2	Transglutaminase 2 (C polypeptide, protein-glutamine-gamma-glutamyltransferase)	↓	NM_004613.2	Hs.517033
	TNFSF10	Tumor necrosis factor (ligand) superfamily, member 10	↓	NM_003810.3	Hs.478275
	BNIP3	BCL2/adenovirus E1B 19kDa interacting protein 3	↓	NM_004052.2	Hs.144873
	MAPK9	Mitogen-activated protein kinase 9	↓	NM_002752.4	Hs.484371
	FOS	FBJ murine osteosarcoma viral oncogene homolog	↓	NM_005252.3	Hs.25647
	EGR1	Early growth response 1	↓	NM_001964.2	Hs.326035
	JUN	Jun B proto-oncogene	↓	NM_002229.2	Hs.25292
	UBD	Ubiquitin D	↓	NM_006398.3	Hs.44532
	CTGF	Connective tissue growth factor	↓	NM_001901.2	Hs.410037
	EBI3	Epstein-Barr virus induced 3	↓	NM_005755.2	Hs.501452
	HSD3B7	Hydroxy-delta-5-steroid dehydrogenase, 3 beta- and steroid delta-isomerase 7	↓	NM_025193.3	Hs.460618
	MSX1	Msh homeobox 1	↓	NM_002448.3	Hs.424414
	UBE4B	Ubiquitination factor E4B	↓	NM_001105562.2	Hs.593974
	CHD6	Chromodomain helicase DNA binding protein 6	↓	NM_032221.3	Hs.740645
	DDR1	Discoidin domain receptor tyrosine kinase 1	↓	NM_001954.4	Hs.631988
	CD83	CD83 molecule	↓	NM_004233.3	Hs.595133
	MAML2	Mastermind-like 2 (Drosophila)	↓	NM_032427.1	Hs.745167
	UBE2H	Ubiquitin-conjugating enzyme E2H	↓	NM_003344.3	Hs.643548
	SDC4	Syndecan 4	↓	NM_002999.3	Hs.632267
	TCEA2	Transcription elongation factor A (SII), 2	↓	NM_003195.4	Hs.505004
	CPD	Carboxypeptidase D	↓	NM_001304.4	Hs.446079
	RIN2	Ras and Rab interactor 2	↓	NM_001242581.1	Hs.472270

	CXCL16	Chemokine (C-X-C motif) ligand 16	↓	NM_022059.2	Hs.745037
	SLC11A2	Solute carrier family 11 (proton-coupled divalent metal ion transporters), member 2	↓	NM_001174125.1	Hs.505545
	BMF	Bcl2 modifying factor	↓	NM_001003940.1	Hs.591104
	LTB	Lymphotoxin beta (TNF superfamily, member 3)	↓	NM_002341.1	Hs.376208
	RBMS1	RNA binding motif, single stranded interacting protein 1	↓	NM_016836.3	Hs.470412
MAPK	**DUSP1**	Dual specificity phosphatase 1	↓	NM_004417.3	Hs.171695
	JUN	Jun B proto-oncogene	↓	NM_002229.2	Hs.25292
	EGR1	Early growth response 1	↓	NM_001964.2	Hs.326035
	FOS	FBJ murine osteosarcoma viral oncogene homolog	↓	NM_005252.3	Hs.25647
	MAP2K1	Mitogen-activated protein kinase kinase 1	↓	NM_002755.3	Hs.145442
	DLK1	Delta-like 1 homolog (Drosophila)	↓	NM_003836.5	Hs.533717
	CDK4	Cyclin-dependent kinase 4	↓	NM_000075.3	Hs.95577
	ABCB7	ATP-binding cassette, sub-family B (MDR/TAP), member 7	↓	NM_004299.4	Hs.370480
	CDKN1B	Cyclin-dependent kinase inhibitor 1B (p27, Kip1)	↓	NM_004064.3	Hs.238990
	NRAS	Neuroblastoma RAS viral (v-ras) oncogene homolog	↓	NM_002524.4	Hs.486502
	MAP4K3	Mitogen-activated protein kinase kinase kinase kinase 3	↓	NM_003618.3	Hs.655750
	MAPK6	Mitogen-activated protein kinase 6	↓	NM_002748.3	Hs.411847
	TIMP3	TIMP metallopeptidase inhibitor 3	↓	NM_000362.4	Hs.644633
	MAPK9	Mitogen-activated protein kinase 9	↓	NM_002752.4	Hs.484371
	TP53	Tumor protein p53	↓	NM_000546.5	Hs.437460
	CAT	Catalase	↓	NM_001752.3	Hs.502302
	CHUK	Conserved helix-loop-helix ubiquitous kinase	↓	NM_001278.3	Hs.198998
	HRAS	V-Ha-ras Harvey rat sarcoma viral oncogene homolog	↓	NM_005343.2	Hs.37003
	MAP2K2	Mitogen-activated protein kinase kinase 2	↓	NM_030662.3	Hs.465627
	MEF2D	Myocyte enhancer factor 2D	↓	NM_005920.3	Hs.314327
	ELK1	ELK1, member of ETS oncogene family	↓	NM_001114123.2	Hs.181128
	MAPK3	Mitogen-activated protein kinase 3	↓	NM_002746.2	Hs.861
	MKNK2	MAP kinase interacting serine/threonine kinase 2	↓	NM_017572.3	Hs.515032
	MAP2K2	Mitogen-activated protein kinase kinase 2	↓	NM_030662.3	Hs.465627

EMT	**PCOLCE**	Procollagen C-endopeptidase enhancer	↓	NM_002593.3	Hs.202097
	RNASET2	Ribonuclease T2	↓	NM_003730.4	Hs.529989
	CDH2	Cadherin 2, type 1, N-cadherin (neuronal)	↓	NM_001792.3	Hs.464829
	CD68	CD68 molecule	↓	NM_001251.2	Hs.647419
	RRAS	Related RAS viral (r-ras) oncogene homolog	↓	NM_006270.3	Hs.515536
	COL6A1	Collagen, type VI, alpha 1	↓	NM_001848.2	Hs.474053
	PHGDH	Phosphoglycerate dehydrogenase	↓	NM_006623.3	Hs.487296
	GALK1	Galactokinase 1	↓	NM_000154.1	Hs.407966
	SDC2	Syndecan 2	↓	NM_002998.3	Hs.1501
	ASNS	Asparagine synthetase (glutamine-hydrolyzing)	↓	NM_133436.3	Hs.489207
	IFIT1	Interferon-induced protein with tetratricopeptide repeats 1	↓	NM_001548.4	Hs.20315
cell cycle	**CKS1B**	CDC28 protein kinase regulatory subunit 1B	↑	NM_001826.2	Hs.374378
	CABLES1	Cdk5 and Abl enzyme substrate 1	↑	NM_138375.2	Hs.11108
	OIP5	Opa interacting protein 5	↑	NM_007280.1	Hs.661645
	AURKA	Aurora kinase A	↑	NM_198433.1	Hs.250822
	CDC20	Cell division cycle 20	↑	NM_001255.2	Hs.524947
	CETN2	Centrin, EF-hand protein, 2	↑	NM_004344.1	Hs.82794
	CENPA	Centromere protein A	↑	NM_001809.3	Hs.1594
	CRYAA	Crystallin, alpha A	↑	NM_000394.2	Hs.184085
	CCNA2	Cyclin A2	↑	NM_001237.3	Hs.58974
	CCND3	Cyclin D3	↑	NM_001136017.2	Hs.534307
	FAM83D	Family with sequence similarity 83, member D	↑	NM_030919.2	Hs.726442
	MCM7	Minichromosome maintenance complex component 7	↑	NM_005916.3	Hs.438720
	NCAPG	Non-SMC condensin I complex, subunit G	↑	NM_022346.4	Hs.567567
	PA2G4	Proliferation-associated 2G4, 38kDa	↑	NM_006191.2	Hs.524498
	PSMD14	Proteasome (prosome, macropain) 26S subunit, non-ATPase, 14	↑	NM_005805.5	Hs.740477
	PSMD2	Proteasome (prosome, macropain) 26S subunit, non-ATPase, 2	↑	NM_002808.3	Hs.518464
	SNHG3-RCC1	Regulator of chromosome condensation 1	↑	NM_001048194.2	Hs.469723
	THBS1	Thrombospondin 1	↑	NM_003246.2	Hs.164226

	TFDP1	Transcription factor Dp-1	↑	NM_007111.4	Hs.79353
	UHRF1	Ubiquitin-like with PHD and ring finger domains 1	↑	NM_001048201.1	Hs.108106
	CDK4	Cyclin-dependent kinase 4	↓	NM_000075.3	Hs.95577
	CDKN1B	Cyclin-dependent kinase inhibitor 1B (p27, Kip1)	↓	NM_004064.3	Hs.238990
	DUSP1	Dual specificity phosphatase 1	↓	NM_004417.3	Hs.171695
	HEPACAM	Hepatic and glial cell adhesion molecule	↓	NM_152722.4	Hs.745294
	MAPK6	Mitogen-activated protein kinase 6	↓	NM_002748.3	Hs.411847
	PIM1	Pim-1 oncogene	↓	NM_002648.3	Hs.81170
	MCM4	Minichromosome maintenance complex component 4	↑	NM_005914.3	Hs.460184
	RPRC1	MAP7 domain containing 1	↑	NM_018067.3	Hs.356096
	CCNB1	Cyclin B1	↑	NM_031966.3	Hs.23960
	MCM2	Minichromosome maintenance complex component 2	↑	NM_004526.3	Hs.477481
	MCM6	Minichromosome maintenance complex component 6	↑	NM_005915.5	Hs.444118
	MCM3	Minichromosome maintenance complex component 3	↑	NM_002388.4	Hs.179565
	CDKN1A	Cyclin-dependent kinase inhibitor 1A (p21, Cip1)	↑	NM_000389.4	Hs.370771
	CCNB2	Cyclin B2	↑	NM_004701.3	Hs.194698
proliferation	**TIMP3**	TIMP metallopeptidase inhibitor 3	↓	NM_000362.4	Hs.644633
	APOA5	Apolipoprotein A-V	↓	NM_052968.4	Hs.283923
	G6PC	Glucose-6-phosphatase, catalytic subunit	↓	NM_000151.3	Hs.212293
	HPN	Hepsin	↓	NM_182983.2	Hs.182385
	SERPINE1	Serpin peptidase inhibitor, clade E (nexin, plasminogen activator inhibitor type 1), member 1	↓	NM_000602.4	Hs.414795
	ANG	Angiogenin, ribonuclease, RNase A family, 5	↓	NM_001145.4	Hs.283749
	CDK4	Cyclin-dependent kinase 4	↓	NM_000075.3	Hs.95577
	CDKN1B	Cyclin-dependent kinase inhibitor 1B (p27, Kip1)	↓	NM_004064.3	Hs.238990
	HIF1A	Hypoxia inducible factor 1, alpha subunit (basic helix-loop-helix transcription factor)	↓	NM_001530.3	Hs.597216
	JUN	Jun B proto-oncogene	↓	NM_002229.2	Hs.25292
	NRAS	Neuroblastoma RAS viral (v-ras) oncogene homolog	↓	NM_002524.4	Hs.486502
	TGM2	Transglutaminase 2 (C polypeptide, protein-glutamine-gamma-glutamyltransferase)	↓	NM_004613.2	Hs.517033
	VEGFA	Vascular endothelial growth factor A	↓	NM_001025366.2	Hs.73793

	SERPINA1	Serpin peptidase inhibitor, clade A (alpha-1 antiproteinase, antitrypsin), member 1	↓	NM_000295.4	Hs.525557
	PIM1	Pim-1 oncogene	↓	NM_002648.3	Hs.81170
	TNFSF10	Tumor necrosis factor (ligand) superfamily, member 10	↓	NM_003810.3	Hs.478275
	ABCB7	ATP-binding cassette, sub-family B (MDR/TAP), member 7	↓	NM_004299.4	Hs.370480
	BTG1	B-cell translocation gene 1, anti-proliferative	↓	NM_001731.2	Hs.255935
	IGF2	Insulin-like growth factor 2 (somatomedin A)	↓	NM_000207.2	Hs.272259
	ADA	Adenosine deaminase	↓	NM_000022.2	Hs.654536
	MDK	Midkine (neurite growth-promoting factor 2)	↓	NM_001012334.2	Hs.82045
angiogenesis	**ANG**	Angiogenin, ribonuclease, RNase A family, 5	↓	NM_001145.4	Hs.283749
	ANXA2	Annexin A2	↓	NM_001002858.2	Hs.511605
	CDH2	Cadherin 2, type 1, N-cadherin (neuronal)	↓	NM_001792.3	Hs.464829
	CTGF	connective tissue growth factor	↓	NM_001901.2	Hs.410037
	HIF1A	Hypoxia inducible factor 1, alpha subunit (basic helix-loop-helix transcription factor)	↓	NM_001530.3	Hs.597216
	JUN	Jun B proto-oncogene	↓	NM_002229.2	Hs.25292
	LOX	Lysyl oxidase	↓	NM_002317.5	Hs.102267
	TGM2	Transglutaminase 2 (C polypeptide, protein-glutamine-gamma-glutamyltransferase)	↓	NM_004613.2	Hs.517033
	VEGFA	Vascular endothelial growth factor A	↓	NM_001025366.2	Hs.73793
	SERPINE1	Serpin peptidase inhibitor, clade E (nexin, plasminogen activator inhibitor type 1), member 1	↓	NM_000602.4	Hs.414795
	ANGPT1	Angiopoietin 1	↓	NM_001146.3	Hs.369675
	PLG	Plasminogen	↓	NM_000301.3	Hs.143436
	NRP1	Neuropilin 1	↓	NM_003873.5	Hs.131704
	RAMP2	Receptor (G protein-coupled) activity modifying protein 2	↓	NM_005854.2	Hs.514193
	SDC4	Syndecan 4	↓	NM_002999.3	Hs.632267
cell adhesion	**FREM1**	FRAS1 related extracellular matrix 1	↓	NM_144966.5	Hs.50850
	CDH2	Cadherin 2, type 1, N-cadherin (neuronal)	↓	NM_001792.3	Hs.464829
	CADM1	Cell adhesion molecule 1	↓	NM_014333.3	Hs.370510
	COL7A1	collagen, type VII, alpha 1	↓	NM_000094.3	Hs.476218

CTGF	connective tissue growth factor	↓	NM_001901.2	Hs.410037
HEPACAM	Hepatic and glial cell adhesion molecule	↓	NM_152722.4	Hs.745294
IGFBP7	Insulin-like growth factor binding protein 7	↓	NM_001553.2	Hs.479808
ITGB2	integrin, beta 2 (complement component 3 receptor 3 and 4 subunit)	↓	NM_000211.3	Hs.375957
SPP1	secreted phosphoprotein 1	↓	NM_001040058.1	Hs.313
MMP11	matrix metallopeptidase 11 (stromelysin 3)	↓	NM_005940.3	Hs.143751
TIMP3	TIMP metallopeptidase inhibitor 3	↓	NM_000362.4	Hs.644633
TFPI	Tissue factor pathway inhibitor (lipoprotein-associated coagulation inhibitor)	↓	NM_006287.4	Hs.516578
COL6A1	Collagen, type VI, alpha 1	↓	NM_001848.2	Hs.474053
F5	Coagulation factor V (proaccelerin, labile factor)	↓	NM_000130.4	Hs.30054
TIMP2	TIMP metallopeptidase inhibitor 2	↓	NM_003255.4	Hs.633514
FGG	fibrinogen gamma chain	↓	NM_000509.4	Hs.727584
VTN	vitronectin	↓	NM_000638.3	Hs.2257
FN1	Fibronectin 1	↓	NM_212482.1	Hs.203717
F7	coagulation factor VII (serum prothrombin conversion accelerator)	↓	NM_000131.4	Hs.36989

*gene expression highlighted in bold font showing at least 1.5-fold change in HepG2_PBLD groups compared with that in the control groups.($P<1x10^{-3}$)

Table Legend: Microarray analysis showed that overexpression of PBLD resulted in inactivation of several tumorigenesis-related signaling pathways, including MAPK, NF-κB, EMT, angiogenesis and others listed in detail above.